The use of Ctrl+Z in ship design: removing a bulbous bow

The use of Ctrl+Z in ship design: removing a bulbous bow

F P Arribas[1], S Oyuela[2], A D Otero[3,4], R Sosa[2,3], H R Diaz-Ojeda[5]

[1] ETSIN-UPM, Av. de la Memoria, Madrid 28040, SPN
[2] Universidad de Buenos Aires, Facultad de Ingeniería - CEAN – INTECIN, Av. Paseo Colon, Ciudad de Buenos Aires C1063, ARG
[3] Consejo Nacional de Investigaciones Científicas y Técnicas, Godoy Cruz, Ciudad de Buenos Aires C1425FQC, ARG
[4] Universidad de Buenos Aires, Av. Paseo Colon, Ciudad de Buenos Aires C1063, ARG
[5] Universidad de Las Palmas de Gran Canaria, Instituto Universitario de Sistemas Inteligentes y Aplicaciones Numéricas en Ingeniería, Las Palmas de Gran Canaria 35017, SPN
Production Editor, *Journal of Physics: Conference Series*, IOP Publishing, Dirac House, Temple Back, Bristol BS1 6BE, UK

E-mail: `hectorruben.diaz@ulpgc.es`

Abstract. A bulbous bow is a widely employed feature to enhance the hydrodynamic resistance of ships. More than 95% of the merchant fleet incorporates various types of bulbous bows to reduce wave-making resistance and wave breaking. Bulbous bow is also utilized in smaller vessels like fishing vessels. In certain cases, the initial ship design includes the addition of a bulbous bow by default. In this study, which focuses on a typical Argentinian trawler fishing vessel, we investigate the impact of the bulbous bow on resistance. Taking a reverse approach, we modify the fishing vessel by removing the bulbous bow and we evaluate its hydrodynamics. This research aims to assess the reduction in ship resistance achieved by the bulbous bow under different load conditions and speeds, comparing the vessel with and without the bulbous bow. The numerical analysis uses OpenFOAM, and the results are validated through towing tank experiments. The research demonstrates that the performance of the bulbous bow varies across different conditions, indicating that not always the vessel with a bulbous bow is better.

1. Introduction

When ordering a new ship, one of the critical requirements that must be obtained during its operation is the contract speed. This refers to the specified speed at which the ship must navigate while maintaining a specific power consumption. Significant deviations from the contract speed upon delivery of the ship can lead to penalties and conflicts for the designers. Such variations in powering can have a profound impact on various aspects of ship operations, including stability, profitability, and overall performance. Therefore, the accurate determination of the speed-resistance curve in ship design is of utmost importance.

In the early stages of the ship design, when the hull form is nearly finalized, statistical and regression methods are commonly used for initial estimations. The Holtrop and Mennen regression method [1], which is based on extensive sea trials and towing tank experiments involving more than 200 ship models, has emerged as the most widely employed approach for estimating ship resistance. However, this method tends to yield higher uncertainties when compared to experimental or numerical results. For instance, a study by Bilec and Obreja [2]

founds discrepancies of up to 30% in resistance when comparing the Holtrop-Mennen results with experimental tests for fishing vessels.

As ship design progresses, more accurate and reliable methods are required to account for various shape, viscous, and pressure effects that cannot be adequately addressed through statistical approaches alone. Experimental Fluid Dynamics (EFD) involving towing tank tests has traditionally been the most reliable method in such cases. However, with the rapid advance of computational resources, Computational Fluid Dynamics (CFD) has gained prominence due to its enhanced post-processing capabilities, becoming a reliable alternative [3].

The International Towing Tank Conference (ITTC) regulates the use of these methods through its "Recommended Procedures." These procedures establish guidelines to ensure a consistent methodology for obtaining accurate results, offering rules for both numerical and experimental approaches.

The fishing industry in Argentina has experienced significant transformations since the 1960s. The hake fishery began between 1961 and 1969, followed by the incorporation of fresh fish vessels from 1970 to 1975 to improve catch quality and freshness. Frozen fish processing vessels were introduced between 1976 and 1981, while the 1980s witnessed the development of coastal fisheries and the expansion of the shrimp fishery [4]. In March 2019, a task force was established in Argentina to implement measures aimed to reduce bycatch in fisheries. This task force brings together scientists and stakeholders from both the public and private sectors. Furthermore, Argentina has initiated a fleet modernization process to enhance crew safety and adopt newer, more environmentally sustainable technologies. It is worth noting that more than 50% of the Argentine fleet currently exceeds the recommended age limits set by international standards [5].

In general ship hull design, the inclusion of a bulbous bow below the waterline is a common feature due to its effectiveness in reducing total resistance and installed power, thereby improving the economic efficiency of the design through reducing fuel consumption. A well-designed bulbous bow can lead to favorable interference between the bow waves generated by the bulb and those generated by the hull, resulting in resistance reduction ranging from 12% to 15% [[6], [7]], assuming the vessel maintains a consistent speed. Consequently, this principle guides the design of typical Argentine fishing vessels.

However, an incorrect design can result in a negative interference between these two wave systems, leading to a significant increase in ship resistance. Given the complex interactions between the hull and bulbous bow waves, designs are not universally efficient for all ship speeds and operating conditions, considering the varying load conditions and speeds at which fishing vessels operate. For instance, trawler fishing vessels experience different displacements when traveling to the fishing grounds without load and when returning to port with fish on board. Speeds can also vary depending on external factors such as weather conditions and competition with other fishing vessels trying to reach the same fishing grounds.

The design of a bulbous bow has always been a complex and controversial task. Although model tests involving a wide range of hull forms and bulb shapes have been conducted to select an optimal bulbous bow design with minimal resistance [8], it is not always feasible due to the considerable time and cost involved. In such cases, numerical methods come to the aid of the design process. One of the most renowned experimental studies was carried out by Kracht [9], who tested numerous bulbous bow models and employed statistical analysis of the tests to develop design charts commonly used for bulbous bow design. However, these charts are not applicable to smaller fishing vessels, and if designers use them, the resulting bulbous bows may not be optimal due to the differences between the designed bulb and those used in the tests (which were intended for larger vessels).

Existing studies often rely on model testing based on Kracht charts [10] or [11]. Some studies also employ CFD analysis to optimize design variables such as length, frontal area, breadth, and depth of a bulbous bow. The number of references involving CFD is higher compared to

experimental studies, as presented in works by Peri et al. [12], Sharma and Shenoy [13], Watle and Faltinsen [14].

This work aims to evaluate the efficiency of a bulbous bow for a fishing trawler. To achieve this, authors decided to remove the bulbous bow from the original design, representing a unique and novel approach in ship design. There are no previous references to this inverse procedure, hence the title, a "Ctrl + Z" in the design process. By employing CFD, the study investigates the hydrodynamic behavior of the hull without the bulbous bow. The results provide valuable insights into the range of application of the original bulbous bow design and lay the groundwork for future bulbous bow designs, leveraging the knowledge gained from these studies.

2. Experimental Setup

As mentioned earlier, accurately quantifying ship resistance is crucial in ship design. Towing tank experiments are the conventional method for obtaining the ship resistance-velocity curve. The total resistance is measured at various Froude numbers (Fn) ranging from 0.10 to 0.45.

2.1. Model Ship

For this study, a typical Argentine fishing vessel was selected. A 1:20 scale model of the ship was built using Glass-Fiber Reinforced Plastic (GFRP) for the towing tank experiments. The model was manufactured in accordance with the ITTC recommended procedures [15], paying close attention to model manufacturing tolerances, surface finish, and the size and positioning of turbulence stimulation elements. A trip wire, located at 5% of LPP (Length Between Perpendiculars) aft from the fore perpendicular, was used for turbulence stimulation. Additionally, a wire was employed to promote turbulence at the bulbous bow, situated 1/3 of the bulb length from its fore end. Both wires had a diameter of 1.0 mm. Only the bulbous bow ship model was built and tested to optimize costs.

The main characteristics of the full-scale ship and the ship model with the bulbous bow are shown in Table 1. The characteristics for the case without the bulbous bow are presented in Table 2. To distinguish between the models, the letter "b" is used to represent the case with the model that includes the bulbous bow. A graphical comparison of the ship with and without the bulbous bow can be seen in Figure 1, where the Sectional Area Curves of the two models are compared. The study analyzes three load conditions: ballast condition (ship draught of 3.3 m), full load condition (ship draught of 3.9 m), and an intermediate load condition (ship draught of 3.6 m).

2.2. Towing Tank

The towing tank experiments were conducted in the towing tank at the University of Buenos Aires (UBA), Argentina. The tank, known as the Canal de Experiencias de Arquitectura Naval (CEAN), has dimensions of 72 m in length, 3.6 m in width, and a variable depth of up to 2 m. For this study, the water depth was set at 1.80 m.

The towing tank is equipped with a running carriage capable of reaching a maximum speed of 4.0 m/s. The ship model, properly ballasted to achieve the required displacement and waterline, was attached to the resistance dynamometer. A one-component force transducer of type R 47 manufactured by Kempf & Remmers was used in the dynamometer for resistance tests. Coupling the model to the carriage via the resistance dynamometer prevented surge, yaw, and heel, allowing the model to be free in trim and sinkage. The resistance transducer is designed to handle a full-scale load of ± 100 N and has a sensitivity of approximately ± 1 mV/V of supply voltage.

Table 1. Main parameters of full-scale ship and ship model

Main Particulars	Symbol	Unit	Ship	Model 1b	Model 2b	Model 3b
Model scale	λ	[-]	-	20	20	20
Length on waterline	L_{WL}	[m]	32.68	1.634	1.662	1.641
Length over wetted surface	L_{OWS}	[m]	34.795	1.670	1.740	1.740
Breadth	B	[m]	9.28	0.464	0.464	0.464
Draught	D	[m]	3.30	0.165	0.180	0.195
Displacement volume	∇	[m^3]	599.40	0.075	0.085	0.095
Wetted surface area	S	[m^2]	392.67	0.982	1.058	1.124
Block Coefficient	C_B	[m]	0.60	0.60	0.61	0.64
Midship section area coeff.	C_X	[m]	0.86	0.86	0.87	0.89

Table 2. Main parameters of full-scale ship and ship model without bulbous bow

Main Particulars	Symbol	Unit	Model 1	Model 2	Model 3
Model scale	λ	-	20	20	20
Length on waterline	L_{WL}	[m]	1.515	1.565	1.575
Breadth	B	[m]	0.464	0.464	0.464
Draught	D	[m]	0.165	0.180	0.195
Displacement volume	∇	[m^3]	0.068	0.077	0.087
Wetted surface area	S	[m^2]	0.969	1.049	1.122
Block Coefficient	C_B	[m]	0.58	0.59	0.61
Midship section area coeff.	C_X	[m]	0.86	0.87	0.89

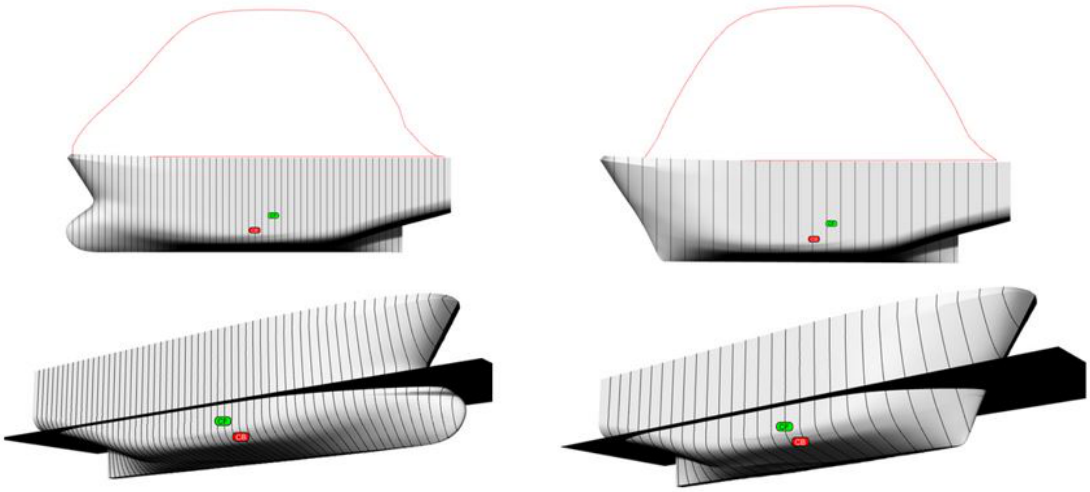

(a) (b)

Figure 1. Comparison in light condition. a: original model, b: without bulbous bow

The mid-sectional area of the vessel is 1%, 1.1%, and 1.2% of the towing tank section area in the ballast, intermediate, and full load conditions, respectively. To account for the blockage effect caused by the presence of the model in the towing tank, Schuster's blockage correction

method is applied following the ITTC (International Towing Tank Conference) procedure [16].

The analysis of uncertainty for the resistance measurements in the towing tank experiments considers several significant uncertainty components. These components include the hull geometry, towing speed, water temperature, calibration of the dynamometer, and repeat tests. The standard uncertainty associated with each component is estimated and then combined using the Root-Sum-Square (RSS) method, as recommended by the ITTC (International Towing Tank Conference) [17].

The uncertainty components related to the hull geometry include the wetted surface area and the representative length of the model, which are estimated in terms of the standard uncertainty of the displacement mass. The uncertainty associated with the hull geometry is quantified by measuring the model ballasting. The resulting uncertainties for different speeds (Fn = 0.14, Fn = 0.26, Fn = 0.37) are presented in Table 3.

Table 3. Combination of uncertainty in measurement for resistance at Fn = 0.14, Fn = 0.26 and Fn = 0.37. Repeat test N = 4

Uncertainty Components	Fn = 0.14	Fn = 0.26	Fn = 0.37
Hull geometry	0.05	0.05	0.05
Speed	0.067	0.067	0.067
Water temp.	0.03	0.03	0.03
Dynamometer	4.73	1.04	0.35
Repeat test, Deviation[a]	5.00	3.50	1.50
Combined for single test	6.88	3.65	1.54
Repeat test, Deviation of mean	2.50	1.75	0.75
Combined for repeat mean	5.35	2.04	0.83
Expanded for repeat mean	10.70	4.08	1.66

[a] Repeat test, Deviation = (Repeat test, Deviation of mean)$*N^{1/2}$

The uncertainty of towing speed affects the resistance measurement through the dynamic pressure and the Reynolds (Re) number. The relative uncertainty of the towing speed, which is limited by the bias of the towing carriage, is considered. The resulting uncertainties in resistance due to velocity are also presented in Table 3.

Water temperature variation has a significant effect on water viscosity, Re number, and frictional drag. The deviation of water temperature during the tests showed a variation of less than 0.5°C. The corresponding uncertainties in resistance due to temperature variation are included in Table 3.

The resistance dynamometer is calibrated before and after each test, and the standard deviation of the linear regression is adopted as the standard uncertainty of calibration. The uncertainties related to the calibration of the dynamometer are presented in Table 3. The uncertainty associated with the weights used for ballasting is considered negligible.

The resistance measurements are obtained using a R47 dynamometer with a sampling rate of 200 Hz. The measurements are averaged over a time interval of at least 10 seconds, and the standard uncertainty of the average of the sampling history is determined. The uncertainty of one reading from the Data Acquisition System (DAS) is considered negligible.

Repetition tests are performed, and the mean of the resistance measurements is adopted as the best estimate. The standard uncertainty of the mean from N repeated tests, with N = 4 in this case, is estimated according to the ITTC procedure [17]. The standard uncertainties for repeat tests are shown in Table 3.

Finally, the significant components of uncertainties are combined using the RSS method, and the results are presented in Table 3. The dynamometer and the precision of measurement are

identified as the major sources of uncertainty in the repeated tests. The uncertainty of resistance measurements decreases with increasing speed, as the contribution from the dynamometer decreases. The expanded uncertainties in Table 3 correspond to a confidence level of 95%. The uncertainty of resistance measurements for Fn = 0.14, Fn = 0.26, and Fn = 0.37 are 5.35%, 2.04%, and 0.83%, respectively.

3. CFD Model

3.1. Numerical Procedure

The use of Computational Fluid Dynamics (CFD) for ship resistance is widespread. OpenFOAM is one of the most commonly used numerical codes in the community. It is a free and open-source tool that implements the well-known Navier-Stokes equations, along with various numerical schemes and procedures used to solve fluid flow problems. Based on the finite volume method, this code considers incompressible Newtonian flow in the present work. Consequently, the equations of interest are the Navier-Stokes mass and continuity equations, represented by Equation 1 and Equation 2.

Due to the presence of turbulence in ship resistance, a turbulence model is necessary. The Reynolds-Averaged Navier-Stokes (RANS) method is employed to model turbulent flow and perform a time-average of flow quantities. This method offers different models, such as SST k-ω, which includes two eddy-viscosity equations. In this model, k represents the turbulent kinetic energy, while ω denotes the specific dissipation rate.

Two different types of simulations were conducted in this study. Firstly, a simulation involving a single fluid in a double hull configuration, and secondly, a simulation with two phases present, as depicted in Figure 2. In the numerical analysis, the previous equation descriptions are utilized when considering only one fluid. However, when both water and air are present as two phases, an equation capable of handling the presence of both fluids is required. The Volume of Fluid (VOF) method, as shown in Equation 3, is employed for this purpose. This method utilizes a scalar volume fraction α ranging between 0 and 1 to indicate the proportion of each phase contained within each fluid cell. Specifically, α takes a value of 0 for air and 1 for water.

$$\nabla \cdot \overline{U_f} = 0 \tag{1}$$

$$\frac{\partial(\rho_f \overline{U_f})}{\partial t} + \nabla(\rho_f \overline{U_f U_f}) = \rho_f g - \nabla p + \mu_f \nabla^2 \overline{U_f} \tag{2}$$

$$\frac{\partial(\alpha)}{\partial t} + \overline{U_f} \cdot \nabla \alpha = 0 \tag{3}$$

3.2. Numerical Domain and Boundary Conditions

The computational domain utilized in the simulations is depicted in Figure 2. To prevent any blockage effects, the distances within the domain have been chosen sufficiently far from the ship model. The boundary conditions applied in the simulations are summarized in Table 4.

3.3. Mesh Convergence

An analysis of mesh convergence was performed for a draft of 0.165 meters, light condition, and a Froude number of 0.45. The results obtained from different meshes were compared to assess convergence. The results are summarized in Table 5. Once a consistent trend in cell number was observed, Mesh 4 was selected as the final mesh for the remaining cases. Figure 3 illustrates the final mesh, Mesh 4, where refined cells are employed to capture accurately the flow around the ship, while a thin refinement is applied to the entire domain to capture the air-water interface.

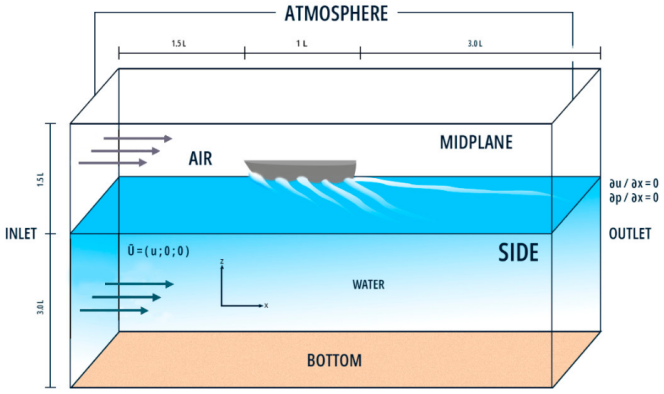

Figure 2. Problem set up and main parameters

Table 4. Boundary conditions

Patch	U	p	k	ω	μ turbulent
Inlet	uniform	fixed flux	fixed value	fixed value	fixed value
Outlet	zero gradient	zero gradient	zero gradient	zero gradient	zero gradient
Atmosphere	zero gradient	zero gradient	zero gradient	zero gradient	zero gradient
Bottom	symmetry	symmetry	symmetry	symmetry	symmetry
Midplane/Side	symmetry	symmetry	symmetry	symmetry	symmetry
Ship	no slip	fixed flux	wall function	wall function	wall function

Table 5. Mesh convergence analysis

Case	Mesh cells	Fn	F [N]	Error (%)
EFD	-	0.45	40.27	-
Mesh 1	633.938	0.45	40.26	0.02
Mesh 2	903.744	0.45	41.76	3.70
Mesh 3	1.213.419	0.45	40.34	0.17
Mesh 4	2.485166	0.45	41.16	2.21

4. CFD Validation

Before analysing the effect produced by removing the bulbous bow in the trawler vessel, an exercise of validation is necessary. Figure 4 shows the non-dimensional total resistance curve (C_T), numerical and experimental, for Froude numbers between 0.1 and 0.45, considering different draughts. A good agreement in C_T between EFD and CFD results is observed for the three studied draughts and the different Froude numbers.

Normally, fishing vessels operate in different conditions and velocities, i.e. when the fishing vessel is leaving port, when it is fishing or when it comes back to port with the fish. Normally, the design criteria are based on the speed to the fishing area and the coming back to port with the capture. For the present case the ship is designed for sailing at $0.25 < \text{Fn} < 0.35$, being the defined operation speed Fn= 0.35. The curves show the typical behaviour for this kind of vessel.

For higher Fn numbers, the slope of the total resistance curve increases continuously, indicating that C_T is increasing at a rate higher than model ship velocity squared. Wave

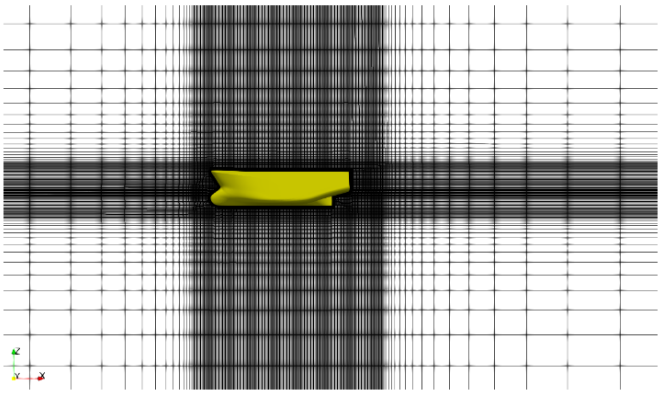

Figure 3. Side view of Mesh 4

resistance is negligible at low speeds, but with increasing velocity, wave resistance grows faster than viscous one. In fact, for most fishing vessels above Fn = 0.30 the wave resistance becomes the largest component of its total resistance, abruptly increasing the ship power and therefore making the vessels inefficient from a consumption point of view.

In ship hydrodynamics it is usual, and useful, to split the wave resistance into two components: wave pattern resistance and wave breaking resistance. If the Fn is large, the waves may be steep enough to break down into eddies and foam. The energy thus removed from the wave system is found in the wake of the ship and the corresponding resistance component is called wave breaking resistance.

The remaining wave energy is radiated away from the ship through the wave system and gives rise to the wave pattern resistance.

The breaking phenomena can be observed in the EFD results for Fn $>$ 0.3, as shown in Figure 5d (Fn = 0.37) and Figure 5f (Fn = 0.45). The CFD results seem to capture the wave breaking phenomena only for the higher Froude number, as seen in Figure 5e (Fn = 0.45). A more detailed description of these phenomena using the CFD model would require a finer mesh in the interface region. However, it is important to note that the wave breaking resistance is considerably smaller than the wave resistance for this type of fishing vessel. From these visualizations, it can be observed that the hull's shoulders play an important role in the distribution of waves along the hull. In this context, it is noticeable that for higher Froude numbers, a maximum hollow wave appears in the ship hull section 14.5 and moves back towards section 11.5 in the case of Fn=0.45.

5. Discussion

Once the numerical procedure is validated, a comparison of force coefficients between the two cases is presented in Figure 6. The calculations for both ships have been conducted for the same draft instead of maintaining a constant displacement value. It should be noted that the lightship weight of the modified ship without the bulbous bow is unknown unless structural calculations are performed. Therefore, in this paper, the draft has been kept the same, resulting in different displacements but maintaining the frontal area of both hulls.

Figure 6 illustrates the comparison for three draughts: a) D1 (0.165 m), b) D2 (0.180 m), and c) D3 (0.195 m), and speeds ranging from Fn = 0.1 to Fn = 0.35.

From Figure 6, it can be observed that for D1 (the lightest draught), the bulbous bow performs better for Fn $>$ 0.25, about 9 knots. This observation seems reasonable since the ship travels to the fishing grounds at higher speeds. However, if the ship operates within the range of Fn [0.2 – 0.25] [7 – 9 knots], the design without a bulbous bow exhibits lower resistance. This

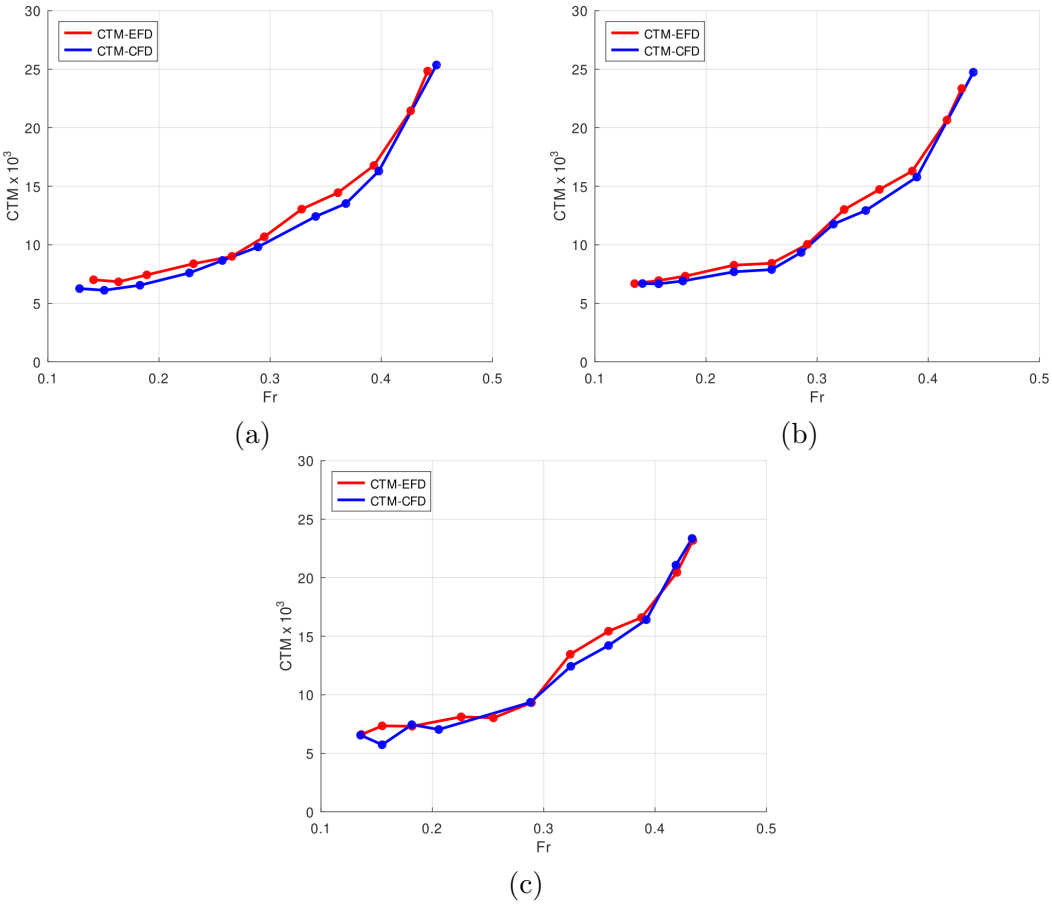

Figure 4. C_T vs Fn for different draughts. a: D1 (0.165 m), b: D2 (0.180 m), c: D3 (0.195 m).

could be advantageous when weather conditions may reduce the ship's speed.

For the intermediate condition D2, the bulbous bow performs worse for Fn < 0.25, which corresponds to speeds lower than 9 knots. Conversely, the bulbous bow improves resistance beyond this range. This observation is particularly interesting as it represents the sailing condition between fishing points. It becomes evident that the bulbous bow works well unless the ship exceeds 9 knots.

For the heavy condition D3, the bulbous bow performs better for Fn > 0.25. However, for lower speeds, it is unclear which hull shape would be better.

Based on the findings from Figure 6, it can be inferred that Fn $= 0.25$ is a critical velocity. Beyond this point, if the speed increases, the bulbous bow yields better performance for the various draughts investigated. At lower speeds, there is uncertainty regarding the better hull shape, as the hull without a bulbous bow occasionally exhibits superior resistance characteristics.

In summary, when incorporating a bulbous bow into a design, careful considerations must be given to the operational speeds. If an economical speed is maintained for a significant portion of the operational time, the bulbous bow may not provide a distinct advantage that becomes apparent at higher speeds. The different loading conditions encountered during operations need to be thoroughly examined, as demonstrated in the intermediate condition D2. Environmental factors, such as sailing in waves, should also be taken into account.

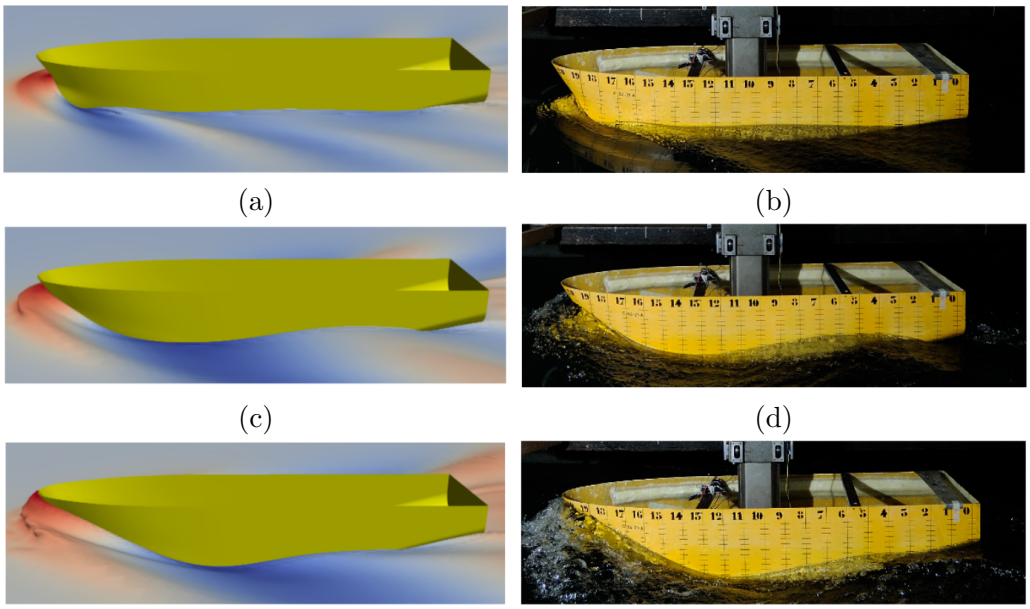

Figure 5. Wave pattern for different Fn and draught = D3. Left column: 3D CFD model. Right column: EFD model. First row: Fn = 0.26, second row: Fn = 0.37, third row: Fn = 0.45.

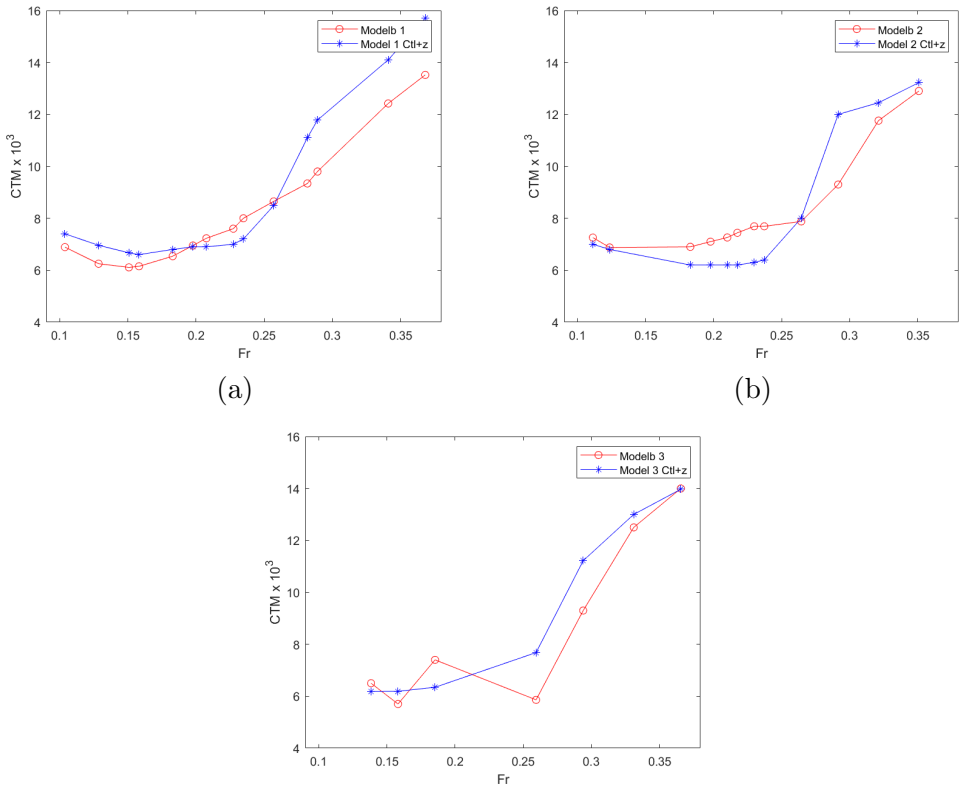

Figure 6. Total drag coefficient comparison for the bulbous bow hull and the case without bulbous bow for three different draughts: a: D1 (0.165 m), b: D2 (0.180 m), c: D3 (0.195 m).

6. Conclusions

Based on the preceding findings, it is evident that a critical point exists at Fn = 0.25. This Froude number represents a critical velocity, as it is uncertain whether the bulbous bow provides superior performance compared to the hull without one at lower velocities for any draught. Conversely, higher speeds clearly demonstrate that the hull with a bulbous bow experiences lower total resistance. This observation may be attributed to wave interference.

Based on the results, it can be deducted that the inclusion of a bulbous bow ideally enhances the ship's performance. However, under adverse sailing conditions or other factors that result in reduced speed, the absence of a bulbous bow becomes a better alternative. Further investigations are required to quantify the performance of different hull shapes under these non-ideal conditions.

References

[1] Holtrop J 1984 *International shipbuilding progress* **31** 272–276
[2] Bilec M and Obreja C D 2020 *IOP Conference Series: Materials Science and Engineering* **916** 012011 ISSN 1757-899X publisher: IOP Publishing
[3] Larsson L, Raven H and Paulling J 2010 *Ship Resistance and Flow* Principles of naval architecture (Society of Naval Architects and Marine Engineers)
[4] Bertolotti M, Verazay G, Pagani A, Errazti E and Buono J 2001 *El mar argentino y sus recursos pesqueros* ISSN 987-20245-0-2
[5] OECD 2021 . Fisheries and Aquaculture in Argentina
[6] Ferreiro L D 2011 *Technology and culture* **52** 335–359
[7] Barrass B 2004 *Ship design and performance for masters and mates* (Elsevier)
[8] Chakraborty S 2017 . What's Importance of Bulbous Bow of Ships, Marine Insight
[9] Kracht A 1978 *Transactions of the Society of Naval Architects and Marine Engineers*
[10] Hoyle J W, Cheng B H and Hays B 1986 *Society of Naval Architects and Marine Engineers-Transactions* **94**
[11] Hagen G e a 1983 . A Guide for Integrating Bow Bulb Selection and Design into the U.S. Navy's Surface Ship Hull Form Development Process, Naval Sea Systems Command Technical Note No. 885-55W-TN0001.
[12] Peri D, Rossetti M and Campana E F 2001 *Journal of ship research* **45** 140–149
[13] Sharma R and Sha O P 2005 *Naval Engineers Journal* **117** 57–76
[14] Watle A 2017 *Flexible Bulbous Bow Design-A Hydrodynamic Study* Master's thesis NTNU
[15] Specialist Committee: Procedures for Resistance P and of 23rd ITTC 2002 P O W T 2002 *ITTC – Recommended Procedures and Guidelines: Model Manufacture, Ship Models* (ITTC)
[16] 26th ITTC Resistance Committee 2011 *ITTC – Recommended Procedures and Guidelines - Resistance Test* (ITTC)
[17] 28th ITTC Quality Systems Group 2017 *ITTC - General Guidelines for Uncertainty Analisys in Resistance Tests* (ITTC)

Acknowledgments

This work was supported by the Ministry of Science, Technology and Innovation of the Argentine Republic (MINCyT - Proyecto de Investigación y Desarrollo Tecnológico de la Iniciativa Pampa Azul - B2) and the Universidad de Buenos Aires, Facultad de Ingeniería (Grant Peruilh). We thank the Argentine shipyard TecnoPesca Argentina for providing the fishing vessel lines.